Transactions of the Indian Institute of Metals, Volume 75, Issue 4, April 2022, pp. 983-995
DOI: 10.1007/s12666-022-02540-6

X-ray Diffraction for the Determination of Residual Stress of Crystalline Materials: An Overview

Arijit Lodh[a], Khushahal Thool[b], Indradev Samajdar[b]*

[a] School of Aerospace, Transport and Manufacturing Cranfield University, Cranfield Bedfordshire MK43 0AL, UK

[b] Department of Metallurgical Engineering and Materials Science, Indian Institute of Technology-Bombay, Mumbai, India

*Corresponding Author email: indra@iitb.ac.in

Abstract

Though there are a variety of experimental techniques available for residual stress measurements, diffraction-based measurements have the unique advantage of estimating the individual components of the residual strain matrix in a crystalline material. This is then converted to residual stresses with appropriate continuum elasticity model(s) and X-ray elastic constants (XEC). In particular, measurements based on electron or neutron diffractions have their complexities or availability issues. The laboratory X-ray diffraction, on the other hand, may provide an easy resource and an effective tool. Such measurements range from two tilt methods to more extended d-sin$^2\psi$ measurements and multiple {hkil} grazing incident X-ray diffraction. Measurements can even be conducted on single-crystals with micro-Laue diffraction and extended to stress ODF (orientation distribution function) calculations. These techniques are unquestionably extremely specialized, where measurement uncertainty plays an important role in the effectiveness plus reproducibility of the data. Unfortunately, standard textbooks or review articles typically describe some, but not all, of the techniques. In this overview, different techniques of X-ray diffraction for the determination of residual stresses in crystalline materials have been summarized. It is hoped that potential users may benefit from the deliberations.

Keywords: Residual Stress, X-ray diffraction, grazing incident X-ray diffraction, micro-Laue diffraction, stress ODF.

Published by Springer. This is the Author Accepted Manuscript.
The final published version (version of record) is available online at DOI:10.1007/s12666-022-02540-6. Please refer to any applicable publisher terms of use.

1. Introduction

When a material or component is subjected to non-uniform elastic-plastic strain gradients, residual stresses may get generated [1–6]. This may happen in all materials, crystalline as well as non-crystalline, and depending on their distribution, can be helpful or deleterious [4, 6–8]. In particular, these self-equilibrating stresses are enabled by variations in mechanical properties (elastic stiffness and Poisson's ratio, for example) and suitable constraints (dislocations and grain boundaries) [4, 7–9]. It is well recognized that no materials, components, or constructions of technological significance are devoid of residual stresses [5, 9–11].

In 1913, W.L. and W.H. Bragg [12] discovered the method to estimate interplanar spacing in crystalline materials. In 1919 Albert Wallace Hull published a paper titled "A New Method of Chemical Analysis". There he pointed out that "…. every crystalline substance gives a pattern; the same substance always gives the same pattern; and in a mixture of substances each produces its pattern independently of the others." This discovery initiated the birth of characterization and identification of polycrystalline phases using x-ray diffraction. It has long been considered as the "unique identity" of materials. Following these, a series of research articles were published, from 1922-30 [13, 14], on the possibility of residual stress determination by X-ray diffraction. Today, X-ray diffraction is routinely extended to quantitative measurements of crystallographic texture and residual stresses in crystalline materials [4, 7, 15]. This manuscript, in particular, provides an overview of X-ray based measurements of residual stresses. However, appreciating such an overview requires a theoretical background on residual stresses, especially their origin and types. This has been included in this introduction.

Residual stress is often defined as stress present in a body which is at equilibrium with surroundings in the absence of external load" [11]. A more lucid picture is elaborated in [7], and Figure 1, which describes the generation of residual stress from 'two-phase composite' material elastic-plastic deformation. In particular, 'a' has gone through an elastic deformation while 'b' is subjected to plastic strain as well. In the absence of constraints, 'a' and 'b' are free to relax fully. The presence of constraints, however, introduces the residual stresses. The residual stresses can also be explained based on their microstructural origin. As shown in Figure 2, a relatively small tensile deformation in hexagonal Zirconium [16] leads to deformation twins and 'minor' orientation gradients (change of color in the orientation maps)

but may also introduce changes in the lattice parameters of the unit cell(s) in individual grain(s), which is also orientation dependent.

In 1914, Heyn [17] pointed out that plastic deformation could lead to heterogeneous residual stress distribution. The reason was attributed to the inherent elastic and plastic anisotropy of individual grains. A diverse range of manufacturing processes[18–22], ranging from actual plastic deformation to thermal and chemical treatments and even phase transformation, and/or applications [21–23] may introduce such heterogeneous elastic-plastic deformation and thus generate or modify the patterns of residual stresses. These patterns are typically generalized, based on their scale of existence [8, 11, 24], as macro and micro residual stresses – see Figure 3. Micro stresses can be further subdivided as intergranular and intragranular residual stresses. Thus, the pattern of residual stress is determined by the summation of all three types of residual stresses [24].

$$\sigma_{RS} = \sigma^{macro} + \sigma^{intergranular} + \sigma^{intragranular} \quad (1)$$

The schematic in Figure 4 shows the microstructural scale of all three types of stress in a material.

Residual stress that spans over a long distance covering many grains is known as macro stress. This is often denoted as type I residual stress or bulk residual stress (σ^I). Many processes (machining, forming, joining, heat-treatment, etc.) may generate type I residual stresses of varying magnitudes and distributions. Several such processes [19, 25], enabling inhomogeneous distribution elastic-plastic strains, are listed in Figure 3. In all these cases, the resulting residual stress states are strongly influenced by the existing geometrical conditions as well as the parameters of the treatments or processes used. Macro residual stresses can also occur as a result of simple elastic-plastic loadings, such as in the case of elastic-plastic bending and elastic-plastic torsion of smooth or notched bars. This is often of interest to design engineers. Mathematically, this residual stress is defined as the mean stress over the material volume of interest (V)

$$\sigma^I = \frac{1}{V}\int_V \sigma_{RS} dV \quad (2)$$

Intergranular or type II residual stress (σ^{II}) varies from grain to grain due to heterogeneity and anisotropy of each grain or phase(s). As shown in Figure 1, after uniaxial elastic-plastic tensile deformation, two phases or grains with differences in yield strength and

elastic modulus will naturally generate type II stresses of tensile and compressive in nature. A more practical example of type II stress is given in reference [26], based on heat treatment of tungsten carbide-cobalt composite. Due to the difference in thermal expansion coefficients, cobalt exhibits a tensile residual stress state which is balanced by the compressive residual stress state in the tungsten carbide. Type-II stress is calculated as the deviation from macro stress over the volume of individual crystallite (or phase) of interest.

$$\sigma^I = \frac{1}{V}\int_V (\sigma_{RS} - \sigma^I)dV \tag{3}$$

Intragranular or type III residual stress (σ^{III}), on the other hand, is related to lattice flaws or defects. The residual stress fields that precede dislocations are a good example [27]. Type III stress is thus the local variation of residual stress inside an individual grain from its grain average (or type II) value. Type III residual stress development occurs due to varying stress fields of individual dislocations, dislocation pile-ups, and other microstructural phenomena of discontinuous nature.

The three separate kinds of residual stresses discussed earlier are more of nomenclature and abstractions. In practicality, any technical parts or components with type I residual stresses also have type II and III stresses. Long-range strain incompatibilities act as the material's source of type I stress. As the elastic and plastic properties vary between grains and phases, type II stresses are generated. On the other hand, Crystal imperfections are responsible for type III stresses. Hardened steel axles and machined metal sheets are two common examples showing this superposition of different stress types. Hardened axles, made of low alloy steel, display a superposition of quenching and transformation and deformation-induced residual stresses. All of them reflect as type I stresses enabled by strain gradients, differences in the specific volumes of austenite and martensite and coefficients of thermal expansion. However, the same hardened axles would also exhibit type II residual stresses as a result of elastic anisotropy as well as yield strength anisotropy [5, 11]. Furthermore, the components would also possess type-III residual stresses by differences in dislocation density and interstitially dissolved carbon atoms in martensite.

2. X-Ray Based Measurements of Residual Stress

There are several techniques to estimate residual stresses. Most of them are, however, focused on measuring type I stresses. Based on the nature of measurement, these techniques can be broadly classified [4, 7, 8] as (a) mechanical methods, (b) methods that involve material property change and (c) diffraction techniques. (a) measures the relaxation of stresses, while (b) estimates some intrinsic physical property (magnetic response, ultrasound velocities, etc.). However, this overview deliberates only on the X-ray diffraction-based measurements of residual stress. It is to be noted that only the diffraction techniques can estimate different components of residual strain or stress tensors. Neutron diffraction is arguably robust and can supply volumetric information. The availability of such equipment is, however, limited. Electron diffraction, especially the electron backscattered diffraction-based cross-correlation [28] and the newly emerging stress measurements in transmission electron microscopy [29, 30], have unquestionable potentials. However, calibrating the experimental data to actual residual strain/stress values and the need for serious expertise remain. On the other hand, X-ray diffraction provides an effective tool for experimental measurements, which can easily be exploited in laboratories. Not only do a range of measurement possibilities and protocols exist (as presented later in this section). There are standards (Example: ASTM E915, ASTM E1426, ASTM E2860, etc.) and protocols for residual stress measurements with XRD. The most important aspect of any such measurement is complete elimination of all alignment errors, which (in any 3 or 4 axes goniometer) is more expertise driven than covered in any protocol. Similarly, use of X-ray optics, detector and stress measurement software are best left to the individual groups. It may be noted that an optimized configuration depends on multiple factors, and may not really be generalized. The hardware and software advances are making this tool reliable and relatively easy to use. This is where the concern begins. There are three limiting factors in any future X-ray based measurements of residual stresses. Firstly, the generator or source would determine the special (and even angular) resolution. Increasing availability of synchrotron or synchrotron like (metal-jet for example) might prove to be a game-changer. Similarly, future developments in X-ray optics and detectors do hold the key for overall scenario of X-ray diffraction, including X-ray based residual stress measurements. This review does not want to speculate on those aspects, but provide the theoretical premise through an overall review. The usage often involves a ‘Blackbox’ approach without a notion about the theory and limitations. This overview is expected to summarize such aspects.

Often the vital component for X-ray based residual stress measurement is a Eulerian cradle. This mechanical construction [4, 7] holds the specimen(s), detector arm and associated hardware and is known as a goniometer. Typically, the goniometer performs in Bragg–Brentano or θ – 2θ configuration and involves either 3 or 4-circle movements. These circles refer to four angles $(\theta, \omega, \psi, \phi)$ defining the relationship between the crystal lattice, incident ray and x-ray detector [4, 6]. As in Figure 5, the angles represent,

θ = Bragg angle,

ω = angle between the incident ray and diffracting surface,

ψ = tilt angle,

ϕ = rotation angle.

The following Cartesian reference frames are distinguished (see also Figure 5) [4, 6]:

The specimen reference frame (S): The S_3 axis is perpendicular to the specimen surface, whereas the S_1 and S_2 axes are parallel to it. If there is a preferred direction inside the plane of the surface, such as the rolling direction in the case of a rolled specimen, the S_1 direction is normally aligned with it. The *principal reference frame* (of the stress tensor) is a specific specimen frame of reference (P). The σ_{11}, σ_{22}, and σ_{33} components of the stress tensor are non-zero in this reference frame.

The laboratory reference frame (L): This frame is chosen so that the L_3 axis and the diffraction vector is aligned. The laboratory frame of reference is the same as the specimen frame of reference when $\phi = \psi = 0$. A superscript [C, S (P), or L] is used to designate the reference frame used to express tensors. The absence of any superscript indicates that an equation is acceptable regardless of the tensor representation reference frame used, but the same reference frame must be used for all tensors inside the equation.

Strain or stress is a tensorial quantity, which requires the specification of nine components [4, 6, 7]. Six of these components are independent in an orthogonal coordinate system. Consider (Figure 5) a unit cube within a homogeneously stressed body at static equilibrium with no distribution of body force (or torque) within the body. Forces will be transmitted by the material surrounding the cube on all six faces of this cube. Because the body is in static equilibrium, the forces acting on mutually parallel faces are equal in magnitude but

opposite in sign. Thus, once the coordinate system (right-handed or left-handed) is determined, only three forces acting on three mutually non-parallel cube faces must be considered (Figure 5). The force acting on any face can be broken down into three components: two within the plane on which it is acting and one normal to that plane. The component of force acting in the normal direction is referred to as the normal force, while the component acting in the plane is referred to as the shear force. These account for the residual strain and stress components in the body.

In the mechanical methods [4, 7, 8], residual stress is measured through the measurement of strain, which is estimated by strain gauge(s). In x-ray diffraction, the interatomic planes act as the strain gauge. Residual stress causes a change in the d-spacing, which translates into both peak profile shift and peak broadening [6, 7]. The Bragg's law ($\lambda = 2dsin\theta$), in particular, indicates that the change in interplanar spacing is reflected as a shift in diffraction angle from the unstressed state value (d_0). This shift is naturally proportional to the magnitude of residual strain [6]. To convert the peak shift into residual strain, the accurate value of the stress-free interplanar spacing, d_0, is needed. This can be experimentally measured [4, 31]. However, such measurements are non-trivial. Easier is to use either d-$sin^2\psi$ method [6] or multiple peak grazing incidence angle X-ray diffraction (GIXRD) for estimating residual strain in polycrystalline material by circumventing direct input of d_0 [6]. The estimated residual strain is then converted to residual stress by using an appropriate continuum elasticity law and XEC values [4, 6]. The examples of residual strain may range from traditional Hooke's law to more involved theories of Reuss, Voight, Eshelby-Kroner, etc., while the XEC values may relate to appropriate isotropic or anisotropic databases for solving residual stress. Of course, the measurements/analysis can be far more challenging with triaxial stress measurements, measurements of single-crystal residual stresses with micro-Laue diffraction and calculating the residual stress distributions in 3-dimensional Euler space – the so call residual stress orientation distribution function (ODF). All these techniques are discussed individually in the following sub-sections.

2.1 d-Sin$^2\psi$ Method

When the material is under stress, elastic strains are produced due to non-equilibrium shift of interatomic planes, which is represented [6] as,

$$\varepsilon = \frac{d-d_0}{d_0} = \frac{\Delta d}{d_0} \quad (4)$$

where d and d_0 denote the interplanar spacing of the material in a stressed and unstressed condition. By X-ray method, one can correlate this shift or deviation by differentiating Bragg's law $\left(\frac{\Delta d}{d_0} = -cot\theta\Delta\theta\right)$ with residual strain. It is important to note the following details for the d-$sin^2\psi$ measurements.

For the rotation angle (ϕ) and the tilt angle (ψ) the interplanar spacing measured from the diffraction peak for a given plane $\{hkl\}$, the strain component can be noted as

$$\varepsilon^{\phi\psi} = \frac{d_{\phi\psi}-d_0}{d_0} \quad \text{----------(5)}$$

where $d_{\phi\psi}$ is the interplanar spacing at any angle (ϕ, ψ) and d_0 is the strain-free or equilibrium lattice spacing. In $d - sin^2\psi$ method, the lattice spacing is measured for multiple ψ tilts and ϕ rotations. The value of interplanar spacing or d_ψ^{hkl} is thus determined for a range of ψ and ϕ values. When the sample is tilted by an angle ψ, the peak position shifts, proportional to residual strain present in the material. The slope of the line is used to determine the residual strain using the following equation [6].

$$\varepsilon_{\phi\psi} = \frac{d_{\phi\psi} - d_0}{d_0} =$$

$$\frac{1}{2}S_2(hkl) \times \left[\left(\sigma_{xx}cos^2\phi + \sigma_{yy}sin^2\phi + \sigma_{xy}sin^2\phi\right)sin^2\psi + \left(\sigma_{xz}cos\phi + \sigma_{yz}sin\phi\right)sin^2\psi + \sigma_{zz}cos^2\psi\right] + S_1(hkl)\left(\sigma_{xx} + \sigma_{yy} + \sigma_{zz}\right) \quad (6)$$

If the terms σ_{xz} and σ_{yz} are both zero the $d - sin^2\psi$ graph will be a straight line. But if either of the terms are non-zero then the d_ψ^{hkl} values at positive and negative ψ will be different. This leads to the splitting of the $d - sin^2\psi$ graph or the so-called ψ-splitting [6]. This is illustrated in Figure 6a. As the depth of penetration is low in laboratory XRD, a bi-axial plane-stress condition can be assumed, ignoring no strain perpendicular to the free surface $(\sigma_{33} = 0)$. Applying elasticity theory for isotropic solid, Eq. (6) becomes [6],

$$\varepsilon^{\phi\psi} = \frac{d_{\phi\psi}-d_0}{d_0} = \frac{1+\nu}{E}(\sigma_{11}cos^2\phi + \sigma_{22}sin^2\phi)sin^2\psi - \frac{\nu}{E}(\sigma_{11} + \sigma_{22}) \quad (7)$$

This is the common X-ray residual strain equation that predicts linear $d_{\phi\psi}$ Vs. $sin^2\psi$ behavior. Experimentally, the lattice spacing is measured for multiple $\pm\psi$ tilts (see Figure 6a) and the experimental data is fitted to a least square line where the slope gives the estimate for residual stress assuming the material constants E and v and unstressed lattice spacing d_0 is known.

The assumption of the non-existence of strain components in the normal direction to sample surface and shear components may not always be true as the ψ-split in the expected linear relationship shows the existence of other strain components for most of the materials. In a similar way, the lattice spacing is measured for multiple $\pm\psi$ tilts with a ϕ rotation at 0°, 45° and 90°. This helps to solve the fundamental equation with other strain components and a full strain tensor can be obtained.

The two-tilt method is a simplified version of standard d-$sin^2\psi$ which is used for quick testing (often with a portable XRD). This method is valid only for a small range of peak shift. This presupposes that the fluctuation of measured d with $sin^2\psi$ is linear from the start. To define d vs. $sin^2\psi$, just two ψ tilts are used in the measurement. Other alterations, which are intended for convenience of calculating, Eq. (7) is rewritten as

$$\frac{\Delta d}{d} = \frac{1+v}{E}\sigma_\phi sin^2\psi - \frac{v}{E}(\sigma_{11} + \sigma_{22}) \tag{8}$$

Between these two ψ-tilts, the phrase $\frac{\Delta d}{d}$ can be stated in terms of the shift in 2θ of the diffracted intensity maximum. Bragg's law, $\lambda = 2dsin\theta$, is differentiated as follows:

$$\frac{\Delta d}{d} = -\frac{cot\theta\Delta 2\theta}{2} \tag{9}$$

Thus, from Eqs. (8,9)

$$\sigma_\phi = K \cdot \Delta 2\theta \tag{10}$$

where $\Delta 2\theta$ is the peak shift. K is called the stress constant and is given by

$$K = \frac{Ecot\theta}{2(1+v)sin^2\psi} \tag{11}$$

The single angle technique is another variation in class that is even less sensitive as the ψ range is restricted by the Bragg angle.

2.2 Multiple Peak Grazing Incidence Diffraction Method

The X-ray diffraction measurement of residual stress is possible for very thin surface-adjacent layers or thin films, when small angles of incidence are used. This has been introduced as the low incident-beam angle diffraction method (LIBAD) by van Acker et al.[32]. Marra et al. [33] subsequently invented the grazing-incidence X-ray diffraction (GIXRD) method. This uses so-called in-plane diffraction geometry, in which the diffraction vector is parallel to the sample surface [6]. The effective sampling volume is constrained to a relatively small volume next to the surface of the specimen when using modest angles of incidence. This results in greater diffracted intensities from this region than when using standard X-ray diffraction techniques. The terms 'grazing-incidence XRD' and 'glancing-incidence XRD' are occasionally used in the literature (see, for example, Noyan et al. [24]) to distinguish between angles of incidence. In GIXRD [34], the angle of incidence is very close to the critical angle for total external reflection (a few tenths of a degree), where the penetration depth is only a few nanometers. In the conventional XRD (example d-$sin^2\psi$) with larger angle of incidence, the penetration depth with laboratory X-ray is typical of the order of a few micrometers.

Standard d-$sin^2\psi$ method involves measurement of lattice spacing for a range of $\pm\psi$ tilts and for a fixed diffraction angle. On the other hand, GIXRD [34–39] uses reflections corresponding to different Bragg angles. Thus, GIXRD is a modified geometry based on classical d-$sin^2\psi$ method, which utilizes the full spectrum of x-ray diffraction. It provides information from thin surface layers since the penetration depth of X-rays is reduced because of modified geometry. The penetration depth can be controlled by changing the incidence angle. The diffraction pattern can be obtained with an Intensity – 2θ scan with a certain incidence angle. In this geometry, the following relationship is obeyed: $\psi = \theta - \omega$; where ω is the angle between the incident ray and diffracting surface, θ is Bragg's angle and ψ is the angle between normal to diffracting plane and normal to specimen surface.

If one assumes residual stress to be axisymmetric about normal to the specimen surface, then following linear elasticity or Hooke's law, one may conclude that,

$$\varepsilon_\psi = cos^2\psi\varepsilon_z + sin^2\psi\varepsilon_x = [(1-\nu)sin^2\psi - 2\nu cos^2\psi]\left(\frac{\sigma_x}{E}\right) = f(\psi)\sigma_x \qquad (12)$$

By changing the grazing incidence angle (ω), a series of ε_ψ and $f(\psi)$ can be obtained. By plotting ε_ψ versus $f(\psi)$, the slope of the line results in σ_x. Figure 6b shows as an example of multiple peak GIXRD measurement.

In contrast to conventional d-$sin^2\psi$ method of stress measurement where the $\theta-2\theta$ scan is performed at a suitable arrangement of the incident ray, sample and goniometer, the "rocking" of x-ray by changing ω gives the desired residual stress with depth profile [34–36]. The main disadvantage of this method is difficulty in the determination of inter-planar spacing for high Bragg's angle peaks. This is because the intensity for Bragg's peaks decreases with increase in the value of Bragg's angle. If high angle peaks cannot be included, this will lead to a reduced range of ψ, and may lead to errors in residual stress measurements.

2.3 Triaxial Stress Analysis

The biaxial stress analysis methods, presented previously in section 2.1, assume that strain components (σ_{13}, σ_{23} and σ_{33}) in the surface normal direction are zero. However, in many circumstances, this assumption may not be correct. ψ-splitting reveals the presence of strain components that were previously overlooked in biaxial stress research [4]. Analysis of ψ -split d versus d-$sin^2\psi$, plots in terms of stresses are similar to the analysis for strains. The terms a_1, a_2 are expressed in terms of stresses:

$$a_1 = \left\{\frac{d_{\phi\psi+} + d_{\phi\psi-}}{2d_0} - 1\right\}$$

$$= \frac{1+v}{E}\{\sigma_{11}cos^2\phi + \sigma_{12}sin2\phi + \sigma_{22}sin^2\phi - \sigma_{33}\}sin^2\psi + \frac{1+v}{E}\sigma_{33} - \frac{v}{E}(\sigma_{11} + \sigma_{22} + \sigma_{33}) \quad (13)$$

$$a_2 = \left\{\frac{d_{\phi\psi+} - d_{\phi\psi-}}{2d_0}\right\} = \frac{1+v}{E}\{\sigma_{13}cos\phi + \sigma_{23}sin\phi\}\, sin|2\psi| \quad (14)$$

The stresses σ_{11}, σ_{12}, σ_{22}, and σ_{33} can thus be calculated using the slope and intercept of a_1 versus $d - sin^2\psi$ for $\phi = 0°, 45°, 90°$, the slope of a_2 vs. $sin|2\psi|$ yields stress σ_{13}, σ_{23} at $\phi = 0°, 90°$, respectively. Once the stress tensor in the sample coordinate system is obtained, it can be transformed to any coordinate system via the tensor transformation rule [4].

If the triaxial stress tensor does not contain σ_{13}, σ_{23} in the irradiated volume, then d vs. $sin^2\psi$ will be linear. If σ_{33} is finite within penetration volume, which is often true, then the stress σ_ϕ determined by the method of biaxial stress analysis will contain an error of magnitude σ_{33}. For the sake of eliminating this error, the following methodology can be utilized:

$$m_{\phi A} = \frac{1+v}{E}\{\sigma_{11}cos^2\phi_A + \sigma_{12}sin2\phi_A + \sigma_{22}sin^2\phi_A - \sigma_{33}\}$$

$$= \frac{1+v}{E}(\sigma_{\phi A} - \sigma_{33}) \quad (15)$$

Similarly, we have

$$m_{\phi A+90} = \frac{1+v}{E}(\sigma_{\phi A+90} - \sigma_{33}) \quad (16)$$

The sum of slopes (Eq. (16)) is equal to

$$m_{\phi A} + m_{\phi A+90} = \frac{1+v}{E}\{\sigma_{11} + \sigma_{22} - 2\sigma_{33}\} \quad (17)$$

The intercept, I, of $(\varepsilon_{33})_{\phi\psi}$Vs. $sin^2\psi$ does not depend on ϕ:

$$I = \left(\frac{1+v}{E}\right)\sigma_{33} - \frac{v}{E}(\sigma_{11} + \sigma_{22} + \sigma_{33}) \quad (18)$$

After solving Eqs.(17,18) together for σ_{33}, the stresses $\sigma_{\phi A}, \sigma_{\phi A+90}$ along with the surface directions $S_{\phi A}, S_{\phi A+90}$ may be calculated using Eqs (15,16) [4]. It is to be noted that measurements of σ_{33} with laboratory XRD is not easy, but can impart critical information on the hydrostatic component and cause of failure [31].

2.4 Method to Estimate Single Crystal Residual Stress Tensor

Intergranular residual stress measurement using micro-Laue x-ray diffraction is non-trivial. Though this has been normally attempted only through synchrotron X-ray [40], recent studies [41–43] have developed the technique for laboratory micro-focused XRD as well. Though this development was based on Bruker D8 Discover™ system with Vantec™ area detector and ~50 μm spot size collimator, this can easily be adopted in other similar (or better) configurations as well. It is imperative to know the prior microstructure and the spatial

coordinates for the grains from electron back scatter diffraction (EBSD) measurements . Using appropriate video feed, the X-ray spot is then placed at the respective grain centers. It is important to achieve appropriate rotation and tilt angles of the goniometer with the highest diffraction spot intensity. In general, EBSD pole figure angles are converted to goniometer convention. However, each set of pole figure angles can have several combinations of rotation and tilt angles, all giving rise to Laue diffraction. During post-processing of data, an iteration needs to be performed and only a combination of angles with the highest intensity is chosen. Following steps are then followed.

For a particular grain, $d_{\phi\psi}$, or d-spacing of a single grain at goniometer angles of θ, ϕ, ψ are obtained from centroid position of integrated Laue diffraction spot (Figure 6c). The strain ($\varepsilon_{\phi\psi}$) is calculated from Eq. (5). $\varepsilon_{\phi\psi}$ is related to the average strains ε_{kl} in specimen coordinate system,

$$\varepsilon_{33}^{\phi\psi} = \frac{d_{\phi\psi} - d_0}{d_0}$$

$$= \varepsilon_{11}cos^2\phi sin^2\psi + \varepsilon_{12}sin2\phi sin^2\psi + \varepsilon_{22}sin^2\phi sin^2\psi + \varepsilon_{33}cos^2\psi + \varepsilon_{13}cos\phi sin2\psi + \varepsilon_{23}sin\phi sin2\psi \quad (19)$$

This equation is the fundamental equation of micro-Laue X-Ray strain measurement. This signifies that at least six independent reflections are needed to solve the linear equations to get full stress tensor. Multiplying this strain tensor with appropriate stiffness tensor, residual stress tensors can be obtained. The procedure is schematically explained in Figure 6c. The reader may refer [41–43] for further details. This data from micro-Laue residual strain or stress measurements can then be used to obtain a comprehensive picture of plastic deformation [43, 44] or stress relief annealing [42], Figure 7, opening new dimensions to the microstructural studies. It is to be noted that present day spot size is limited to minimum 50 μm for commercial instruments. Considering big grains (> 100 μm) in a microstructure, it is possible to go from type I to type II stresses by changing the spot size if following information is available/maintained

i. A prior ebsd scan confirming grain size is more than 100 μm, so centre of the grains can be pointed without influence from grain boundaries.
ii. Location of grain centres from ebsd scan which can be identified in optical camera with help from some fiducial markings.

iii. Calibration of diffraction system ensuring x-ray beam does not change the location during rotation and tilt of stage/specimen.

2.5 Estimating Residual Stress as Orientation Distribution Function

This has been used earlier [45] with laboratory XRD and point detector, and also with synchrotron radiation plus area detector[46]. However, the former [47] is an extremely time-consuming process. The advent of large-angle area detector(s) in laboratory XRD, and the possibility of writing appropriate data extraction plus analysis software codes, makes the technique a real possibility in a laboratory XRD set-up [44]. As shown in Figure 8, pole figure angles can be represented as α and β. On the other hand, the area detector data provides diffraction frames in $\gamma - 2\theta$ (azimuthal angle and Bragg angle [48]) coordinate for different goniometer angles (ω, ψ, ϕ), see Figure 5. Pole figure angles can be calculated from the goniometer angles (ω, ψ, ϕ, γ) as [48],

$$\alpha = sin^{-1}|h_3| = cos^{-1}\sqrt{h_1^2 + h_2^2} \tag{20}$$

$$\beta = \pm cos^{-1}\frac{h_1}{\sqrt{h_1^2+h_2^2}} \quad \begin{matrix} \beta \geq 0^0 \; if \; h_2 \geq 0 \\ \beta \geq 0^0 \; if \; h_2 < 0 \end{matrix} \tag{21}$$

where h_1, h_2 and h_3 are the unit vector components along the sample coordinates and can be deduced as,

$$h_1 = sin\theta(sin\phi\, sin\psi\, sin\omega + cos\phi\, cos\omega) + cos\theta\, sin\phi\, cos\psi\, cos\gamma - cos\theta sin\gamma(sin\phi sin\psi cos\omega - cos\phi sin\omega) \tag{22}$$

$$h_2 = -sin\theta(cos\phi\, sin\psi\, sin\omega - sin\phi\, cos\omega) - cos\theta\, cos\phi\, cos\psi\, cos\gamma - cos\theta sin\gamma(sin\phi\, sin\psi\, cos\omega - cos\phi\, sin\omega) \tag{23}$$

$$h_3 = sin\theta\, cos\psi\, sin\omega - cos\theta\, cos\omega\, cos\psi\, sin\gamma - cos\theta\, cos\gamma\, sin\psi \tag{24}$$

Figure 8 shows a typical area detector measurement. Such measurements provided the peak positions and the peak profiles for different values of γ. Each of these does correspond to $\phi - \psi$ values on the pole figure scheme. There were two ambiguities: (i) area detector signal

of a specific γ -value had a spread of θ and (ii) multiple combinations of goniometer angles provided same pole figure angles.

Taking average values resolves both these issues. Residual strains at different angular locations are then calculated from shifts in peak positions. Taking a large specimen with oscillations may remove all biases from 'limited statistics, or texture and grain size effects. During post-processing of data, each diffraction ring can be divided into appropriate γ intervals, each interval being treated as the central γ value (see Figure 8). For each pole figure position, a suitable 2θ spread about the peak angle needs to be considered. However, as in the case of X-ray texture measurements, very high ψ values of lower intensities need to be avoided. The pole figure data can then be inverted and subjected to inversion and calculation of residual strain or stress ODFs (orientation distribution function), see Figure 9 showing φ_2 = 45, 65 and 90 sections. The measurement time can be reduced by several orders of magnitude, than the earlier studies [47] – 200 h versus a few hours, though the challenge remains in intelligent extraction plus analysis of the area detector data.

2.6 Measurement Uncertainty in X-ray based Determination of Residual Stresses

This is a critical issue in any experimental study, especially for the measurement of residual stress with XRD. It needs to be reminded that the XRD measurements are meant for measuring residual strain and then converting the latter to residual stress values. Both steps, however, may involve significant measurement uncertainty. The former, for example, depends on the accurate and reproducible identification of peak position θ [24, 42]. There are four potential inaccuracies in this. Firstly, the spread of X-ray on the incident X-ray or θ_1. Unquestionably synchrotron may provide minimum spread on wavelength and hence lowest θ_1, but this is often not a practical solution. A check on available X-ray sources [48] indicates that the so-called micro-source with suitable X-ray mirrors can provide very low θ_1 as well. θ_2 arises from the incident and diffracted side of the X-ray, and again a choice of suitable X-ray optics does exist. θ_4 depends on the detector. Choice of X-ray detectors is often commercial in nature. However, the user needs to be prudent in making the right choice. For example, in point detectors, two choices are scintillator or gas proportional counter – the latter providing lower energy spread and hence better accuracy. Similarly, available line and area detectors need to be judiciously evaluated to estimate possible errors. The strongest error, however, comes from

the goniometer – the θ_3. This looks counterintuitive, as the modern goniometer with optical grating is known to provide reproducibility of 0.0001°. The problem in θ_3, however, comes from the alignment. XRD alignment for a 3 or 4-axis goniometer demands that all axes of rotations must coincide with the point of contact of the X-ray beam. In a simpler powder diffractometer, this is achieved by adjusting the height by various means (instrumented laser to ½ X-ray intensity calibration and mechanical screw-gauge alignment). In Eulerian cradles, this is far more complicated. It has been the experience of the present authors that even the so-called experienced users are often unaware of θ_3 corrections, and their extracted data may often be questionable.

A significant problem may also arise from identifying the exact peak position. There are several equations [49] to fit an X-ray peak. Unfortunately, the shape of the peak, or peak profile, depends on the nature and configuration of the defects present [50]. This cannot be generalized. There are two choices, use of user judgment or use of intelligent software. The latter has emerged over last one decade as commercial products but are still not perfect. Use of user judgment plus appropriate software is advisable. It is to be noted that even in a fully aligned machine, a wrong algorithm for peak position determination can give rise to significant errors in measurement.

X-ray diffraction leads to the measurement of residual strains. This is then converted to residual stress. The conversion depends on the continuum elasticity model plus XEC database [51]. Wrong combination(s) can give absolutely meaningless data. For example, for textured material with non-linear d-$sin^2\psi$ s the user must use Reuss and high angle {hhh} or {h00} pole [37]. Comparison between different poles has no meaning. In such a case, it is advisable to use multiple {hkil} GIXRD method. Use of wrong or inappropriate XEC database can also give out meaningless data. For example, appropriate values of elastic stiffness tensor are needed and also the user must use anisotropic XEC whenever possible. Finally, sample preparation is important. It is important to note that there are no fundamentally differences between types I, II and III stresses. It depends on the area and the existence of constraints. In other words, XRD measures residual stresses over an area provided constraints are not removed or altered. More specifically, sectioning of the sample and removal of constraints are important, which are dependent on both sample area and sample preparation. Cutting by electro-discharge machining and sample preparation through electropolishing or colloidal silica polishing or chemical etching are needed. If all protocols are strictly adhered to and the diffractometer is

extremely well aligned, the experimental results emerging are going to be both reliable and reproducible.

3. Concluding Remarks

The traditional approach to the microstructure of polycrystalline material (As shown in Figure 10) involves the size and shape of grains, phases and defects. However, a complete understanding requires information on the orientation of the unit cells and their distortion. that can be accomplished by X-ray diffraction based measurements. .

For any comprehensive study of microstructure, quantification of residual stress data is needed.. X-ray diffraction offers an adequate tool for the determination of residual stresses . This overview points out many possibilities and available techniques for such studies. It has also been emphasized that any experimental measurement of residual stresses has significant challenges involving the reliability of such measurements and reproducibility of the experimental data. This overview points out all the techniques of X-ray based residual stress measurements and then moves on to summarize the factors affecting the accuracy and reliability of experimental results. It is hoped that these details will be useful to researchers and practicing engineers – attempting to harness this last frontier of microstructural studies.

Appendix

Residual stress and Ewald Sphere construction

Let's consider (see Fig 11) the diffracting crystal at the centre of Ewald sphere of 1/λ with incident beam entering from point A satisfying Bragg's law. B defines the origin of reciprocal lattice. At no stress state condition, diffracted beam exits from point D. Therefore, length of vector DB is equal to $^1/_{d_{hkl}}$. According to state of residual stress, diffraction peak will shift. Assuming compressive state here for the same crystal, diffracted beam now exits from point C and length of vector CB is equal to $^1/_{d_{hkl,RS}}$. The length difference between vector DB and CB arises from residual stress.

References

1. Heindlhofer K (1948) Evaluation of residual stress. McGraw-Hill Book Company
2. Osgood WR (1954) Residual stresses in metals and metal construction. Reinhold Publishing Corporation
3. Almen JO, Black PH (1963) Residual stresses and fatigue in metals. McGraw-Hill
4. Noyan IC, Cohen JB (2013) Residual stress: measurement by diffraction and interpretation. Springer
5. Withers PJ a HKDH BHADESHIA. Residual stress. Part 1:355–365
6. Cullity BD (1956) Elements of X-ray Diffraction. Addison-Wesley Publishing
7. Verlinden B, Driver J, Samajdar I, Doherty RD (2007) Thermo-mechanical processing of metallic materials. Elsevier
8. Schneider E, Hauk V (1997) Structural and residual stress analysis by nondestructive methods. Amsterdam: Elsevier 522–563
9. Macherauch E (2014) Introduction to residual stress. Advances in surface treatments 4:1–36
10. van Houtte P, de Buyser L (1993) The influence of crystallographic texture on diffraction measurements of residual stress. Acta metallurgica et materialia 41:323–336
11. Withers PJ, Bhadeshia H, Withers PJ, Bhadeshia H (2016) Residual stress. Part 1–Measurement techniques Residual stress Part 1–Measurement techniques
12. Bragg WL (1913) The structure of some crystals as indicated by their diffraction of X-rays. Proceedings of the Royal Society of London Series A, Containing papers of a mathematical and physical character 89:248–277
13. AF Ioffe and M. Kirpitcheva 1922. Phil Mag 43:204
14. Aksenov GJ (1929) Measurement of elastic stress in a fine grained material. Appl Phys(USSR), 6 (1929) 3 16:
15. Rossini NS, Dassisti M, Benyounis KY, Olabi A-G (2012) Methods of measuring residual stresses in components. Materials & Design 35:572–588
16. Thool K, Patra A, Fullwood D, Krishna KVM, Srivastava D, Samajdar I (2020) The role of crystallographic orientations on heterogeneous deformation in a zirconium alloy: A combined experimental and modeling study. International Journal of Plasticity 133:102785
17. Heyn E (1914) Internal strains in cold-wrought metals, and some troubles caused thereby. Journal of the Institute of Metals 12:1–37
18. Creţu SS, Popinceanu NG (1985) The influence of residual stresses induced by plastic deformation on rolling contact fatigue. Wear 105:153–170
19. Wawszczak R, Baczmański A, Braham C, Seiler W, Wróbel M, Wierzbanowski K, Lodini A (2011) Residual stress field in steel samples during plastic deformation and recovery processes. Philosophical Magazine 91:2263–2290

20. Ortiz AL, Tian JW, Villegas JC, Shaw LL, Liaw PK (2008) Interrogation of the microstructure and residual stress of a nickel-base alloy subjected to surface severe plastic deformation. Acta Materialia 56:413–426

21. Bruno G, Ceretti M, Girardin E, Giuliani A, Manescu A (2004) Relaxation of residual stress in MMC after combined plastic deformation and heat treatment. Scripta materialia 51:999–1004

22. Carpenter K, Tabei A (2020) On residual stress development, prevention, and compensation in metal additive manufacturing. Materials 13:255

23. Zijlstra G, Groen M, Post J, Ocelík V, de Hosson JTM (2016) On the role of the residual stress state in product manufacturing. Materials & Design 105:375–380

24. Noyan IC, Huang TC, York BR (1995) Residual stress/strain analysis in thin films by X-ray diffraction. Critical Reviews in Solid State and Material Sciences 20:125–177

25. Wang Z, Gong B (2002) Residual stress in the forming of materials. Handbook of residual stress and deformation of steel 141–149

26. Bock H (1976) Mechanische Eigenschaften von Wolframkarbid-Kobalt-Legierungen

27. Thomas G (1963) Electron microscopy and strength of crystals

28. Jiang J, Britton TB, Wilkinson AJ (2013) Mapping type III intragranular residual stress distributions in deformed copper polycrystals. Acta Materialia 61:5895–5904

29. Byeon JW, Liu J, Hopkins M, Fischer W, Garimella N, Park KB, Brady MP, Radovic M, El-Raghy T, Sohn YH (2007) Microstructure and Residual Stress of Alumina Scale Formed on Ti2AlC at High Temperature in Air. Oxidation of Metals 68:97–111 . https://doi.org/10.1007/s11085-007-9063-0

30. Jain L, Bajpai R, Basu R, Misra DS, Samajdar I (2017) Delamination/rupture of polycrystalline diamond film: defining role of shear anisotropy. Crystal Growth & Design 17:1514–1523

31. Kumar G, Kanjarla AK, Lodh A, Singh J, Singh R, Srivastava D, Dey GK, Saibaba N, Doherty RD, Samajdar I (2016) Burst ductility of Zirconium clads: The defining role of residual stress. Metallurgical and Materials Transactions A 47:3882–3896

32. van Acker K, de Buyser L, Celis J-P, van Houtte P (1994) Characterization of thin nickel electrocoatings by the low-incident-beam-angle diffraction method. Journal of applied crystallography 27:56–66

33. Marra WC, Eisenberger P, Cho AY (1979) X-ray total-external-reflection–Bragg diffraction: A structural study of the GaAs-Al interface. Journal of Applied Physics 50:6927–6933

34. Peng J, Ji V, Seiler W, Tomescu A, Levesque A, Bouteville A (2006) Residual stress gradient analysis by the GIXRD method on CVD tantalum thin films. Surface and Coatings Technology 200:2738–2743

35. Kohli D, Rakesh R, Sinha VP, Prasad GJ, Samajdar I (2014) Fabrication of simulated plate fuel elements: Defining role of stress relief annealing. Journal of Nuclear Materials 447:150–159

36. Welzel U, Ligot J, Lamparter P, Vermeulen AC, Mittemeijer EJ (2005) Stress analysis of polycrystalline thin films and surface regions by X-ray diffraction. Journal of Applied Crystallography 38:1–29

37. Mukherjee D, Tewary U, Kumar S, Karagadde S, Verma RK, Sambandam M, Samajdar I (2020) Imposed thermal gradients and resultant residual stresses: physical and numerical simulations. Materials Science and Technology 36:1020–1036 . https://doi.org/10.1080/02670836.2020.1746537

38. Kumar G, Kanjarla AK, Lodh A, Singh J, Singh R, Srivastava D, Dey GK, Saibaba N, Doherty RD, Samajdar I (2016) Burst Ductility of Zirconium Clads: The Defining Role of Residual Stress. Metallurgical and Materials Transactions A: Physical Metallurgy and Materials Science 47: . https://doi.org/10.1007/s11661-016-3526-3

39. Kumar G, Lodh A, Singh J, Singh R, Srivastava D, Dey GK, Samajdar I (2017) Experimental characterization and finite element modeling of through thickness deformation gradient in a cold rolled zirconium sheet. CIRP Journal of Manufacturing Science and Technology 19:176–190 . https://doi.org/10.1016/J.CIRPJ.2017.09.002

40. Su R, Li L, Wang YD, Nie ZH, Ren Y, Zhou X, Wang J (2018) Intergranular stress study of TC11 titanium alloy after laser shock peening by synchrotron-based high-energy X-ray diffraction. AIP Advances 8:55126

41. Lodh A, Tak TN, Prakash A, Guruprasad PJ, Hutchinson C, Samajdar I (2017) Relating Residual Stress and Substructural Evolution During Tensile Deformation of an Aluminum-Manganese Alloy. Metallurgical and Materials Transactions A: Physical Metallurgy and Materials Science 48: . https://doi.org/10.1007/s11661-017-4280-x

42. Lodh A, Tak TN, Prakash A, Guruprasad PJ, Keralavarma SM, Benzerga AA, Hutchinson C, Samajdar I (2019) Microstructural Origin of Residual Stress Relief in Aluminum. Metallurgical and Materials Transactions A: Physical Metallurgy and Materials Science 50: . https://doi.org/10.1007/s11661-019-05421-8

43. Lodh A, Tewary U, Singh RP, Tak TN, Prakash A, Alankar A, Guruprasad PJ, Samajdar I (2018) Orientation-Dependent Developments in Misorientation and Residual Stress in Rolled Aluminum: The Defining Role of Dislocation Interactions. Metallurgical and Materials Transactions A: Physical Metallurgy and Materials Science 49: . https://doi.org/10.1007/s11661-018-4964-x

44. Lodh A, Tak TN, Prakash A, Guruprasad PJ, Hutchinson C, Samajdar I (2017) Relating residual stress and substructural evolution during tensile deformation of an aluminum-manganese alloy. Metallurgical and Materials Transactions A 48:5317–5331

45. Kallend JS, Huang YC (1984) Orientation dependence of stored energy of cold work in 50% cold rolled copper. Metal science 18:381–386

46. Dorman M, Toparli MB, Smyth N, Cini A, Fitzpatrick ME, Irving PE (2012) Effect of laser shock peening on residual stress and fatigue life of clad 2024 aluminium sheet containing scribe defects. Materials Science and Engineering: A 548:142–151

47. Sahoo SK, Hiwarkar VD, Krishna KVM, Samajdar I, Pant P, Pujari PK, Dey GK, Srivastav D, Tiwari R, Banerjee S (2010) Grain fragmentation and twinning in deformed Zircaloy 2: Response to positron lifetime measurements. Materials Science and Engineering: A 527:1427–1435

48. He BB (2018) Two-dimensional X-ray Diffraction. John Wiley & Sons

49. Borbély A, Groma I (2001) Variance method for the evaluation of particle size and dislocation density from x-ray Bragg peaks. Applied Physics Letters 79:1772–1774

50. Ungár T, Borbély A (1996) The effect of dislocation contrast on x-ray line broadening: a new approach to line profile analysis. Applied Physics Letters 69:3173–3175

51. Vermeulen AC (2001) An elastic constants database and XEC calculator for use in XRD residual stress analysis. Advances of X-ray Analysis 44:128–133

List of Figures

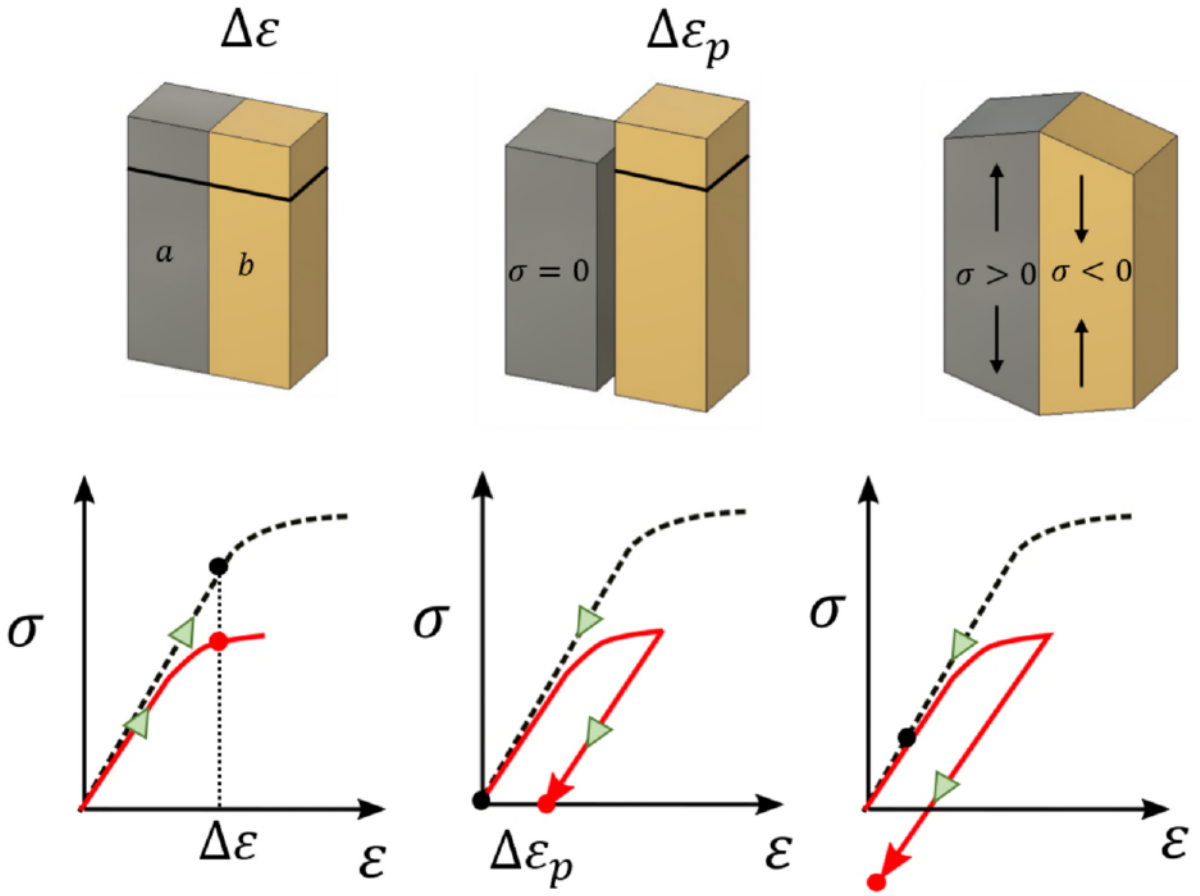

Fig 1: Schematics describing the creation of residual stress by deformation of a two body system (a + b) with different mechanical properties

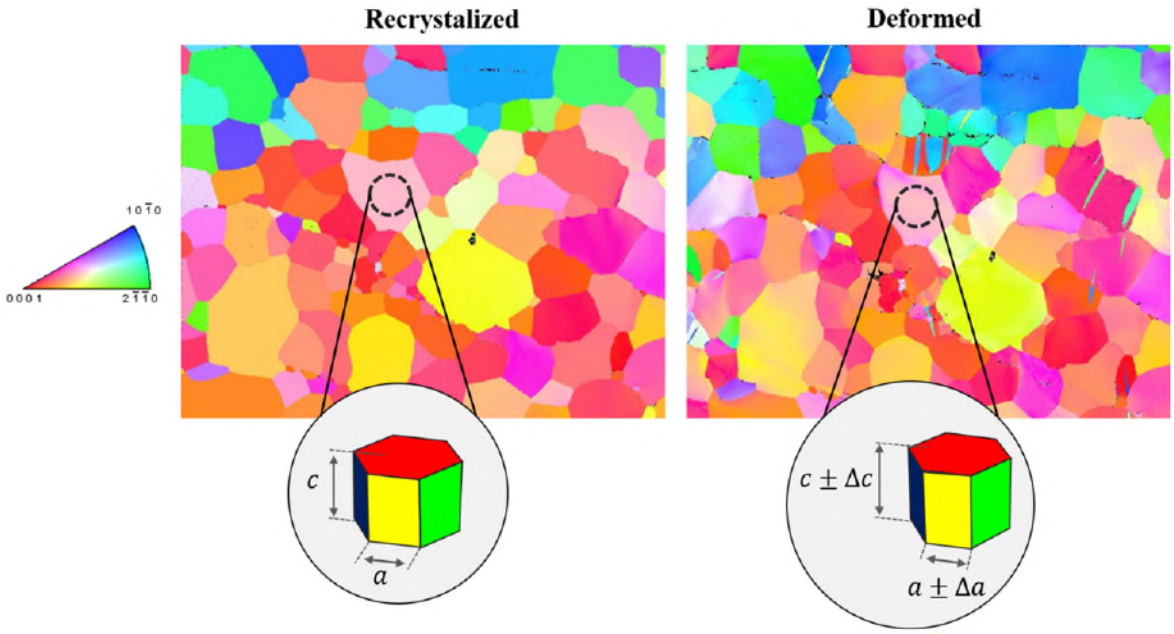

Fig 2: Atomistic origin of residual stress creation from lattice deformation

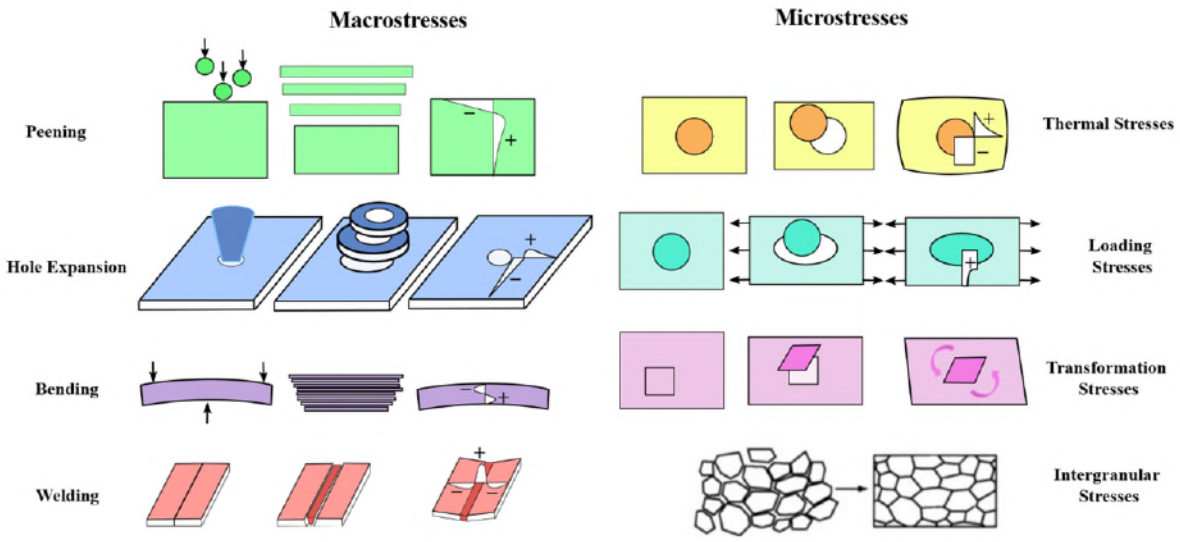

Fig 3: Residual stress origin–micro and macro stresses

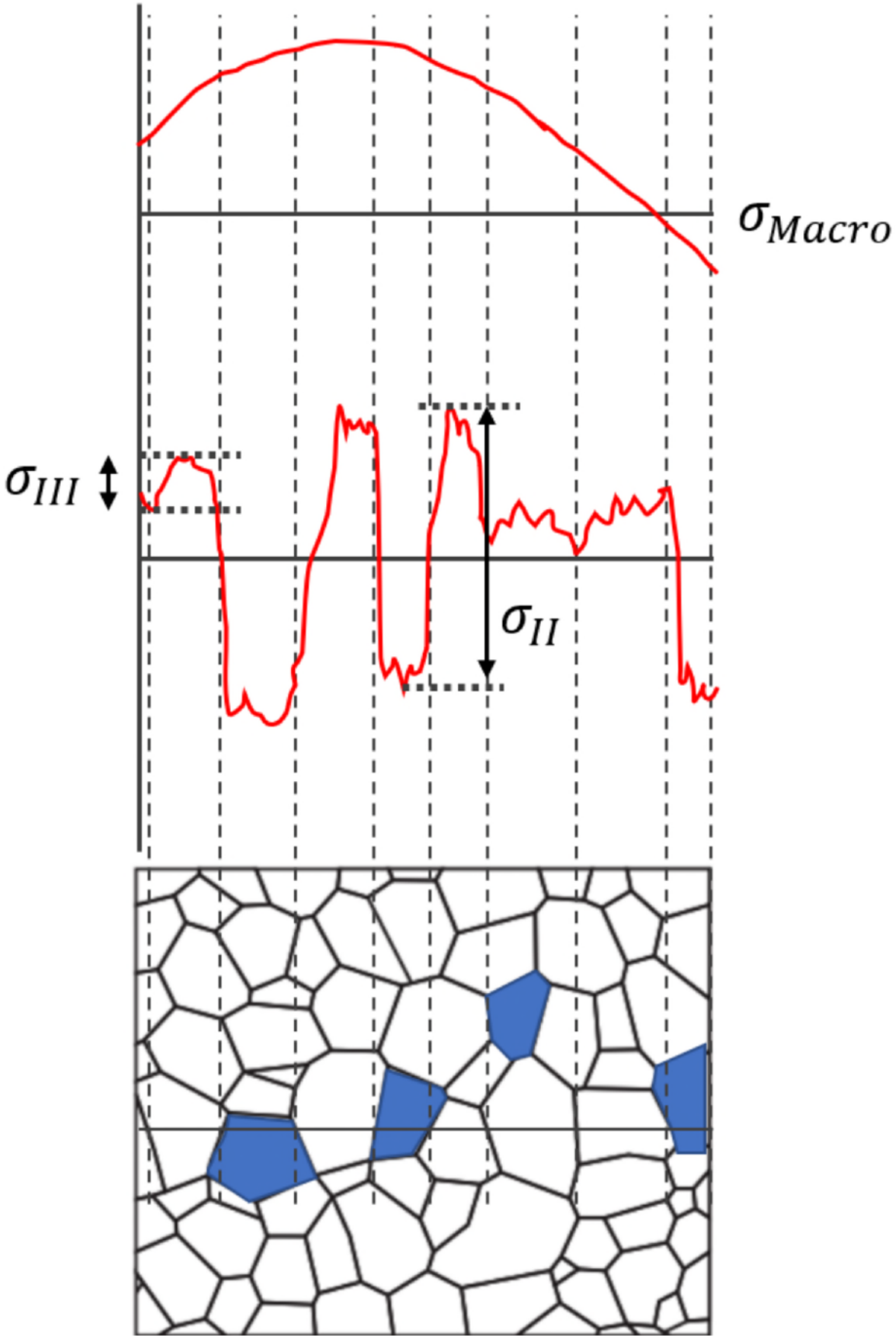

Fig 4: Residual stress fields categorized according to characteristic length scales

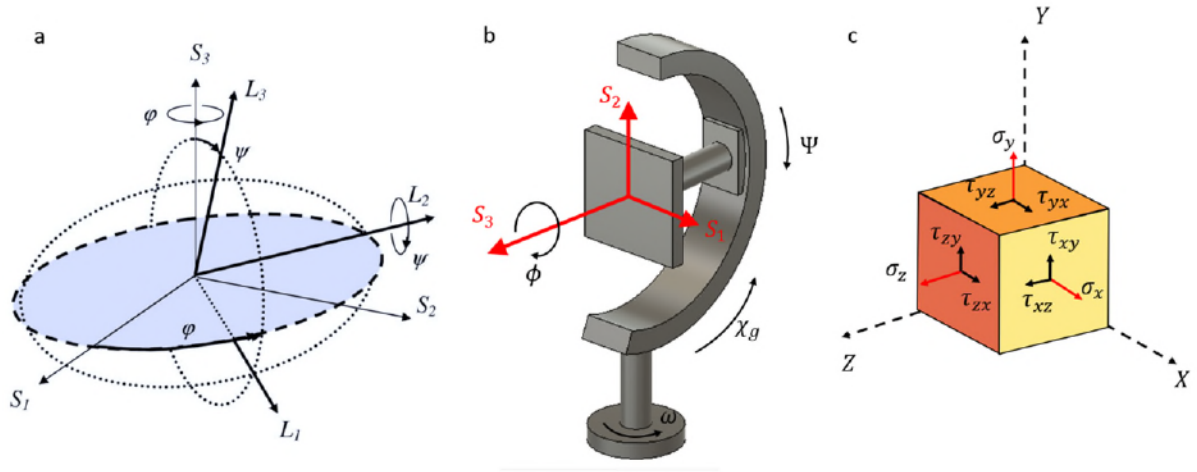

Fig 5: (a) Definition of, and relations between, the sample (S) and laboratory (L) reference frames (b) X-ray system configuration angles, and c general stress convention

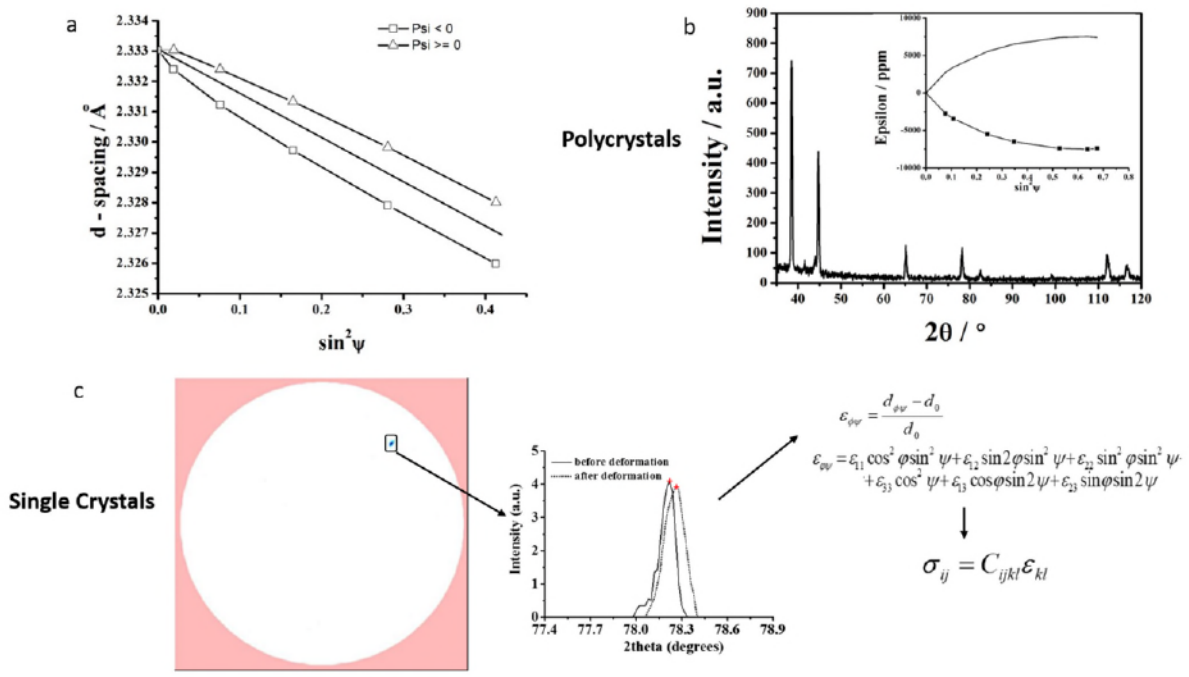

Fig 6: X-ray measured residual stresses for different microstructural length scales (a) Standard d-$\sin^2\psi$ plot with splitting behavior (b) Multiple peak GIXRD measurement for a polycrystalline material (c) Single-crystal stress measurement with micro-focus XRD with an area detector image of a Laue spot from the same grain before and after plastic deformation. A corresponding intensity-2θ plot is also shown

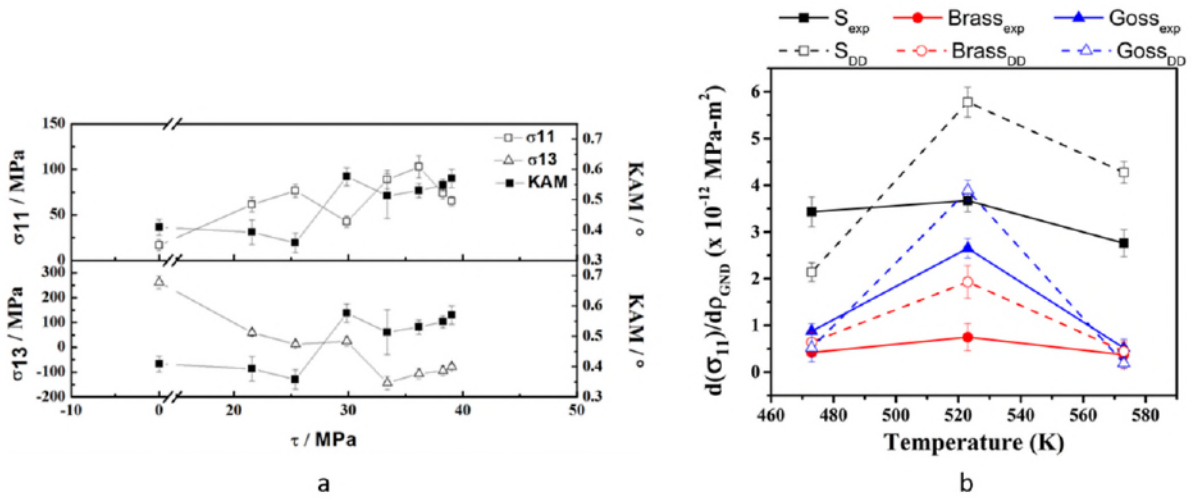

Fig 7: Dislocation substructural evolution and residual stress in (a) tensile deformation and (b) thermal annealing

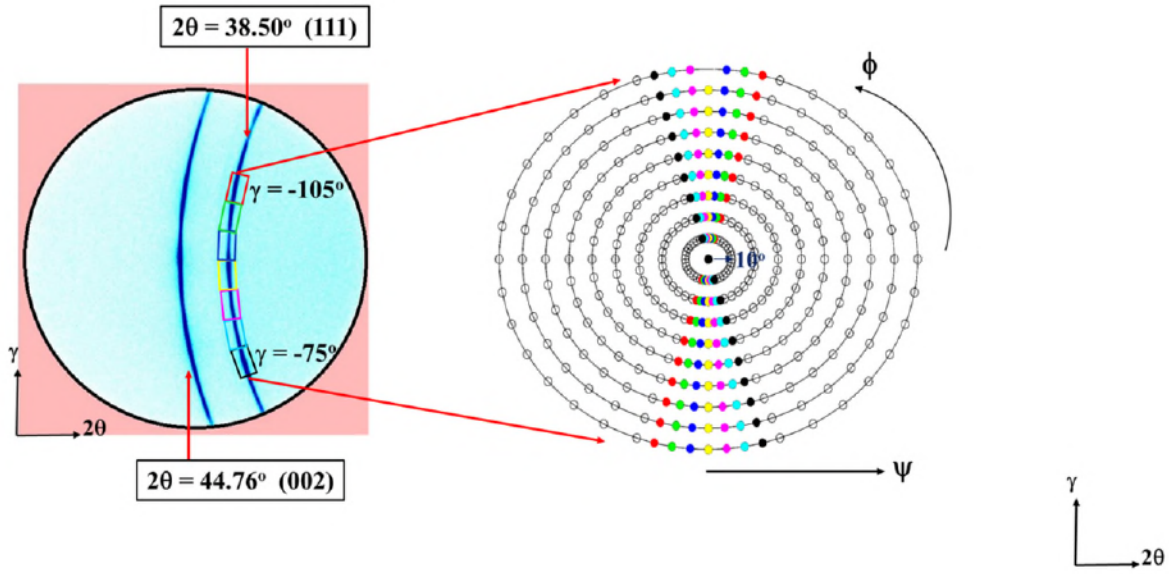

Fig 8: Residual stress measurement in orientation space

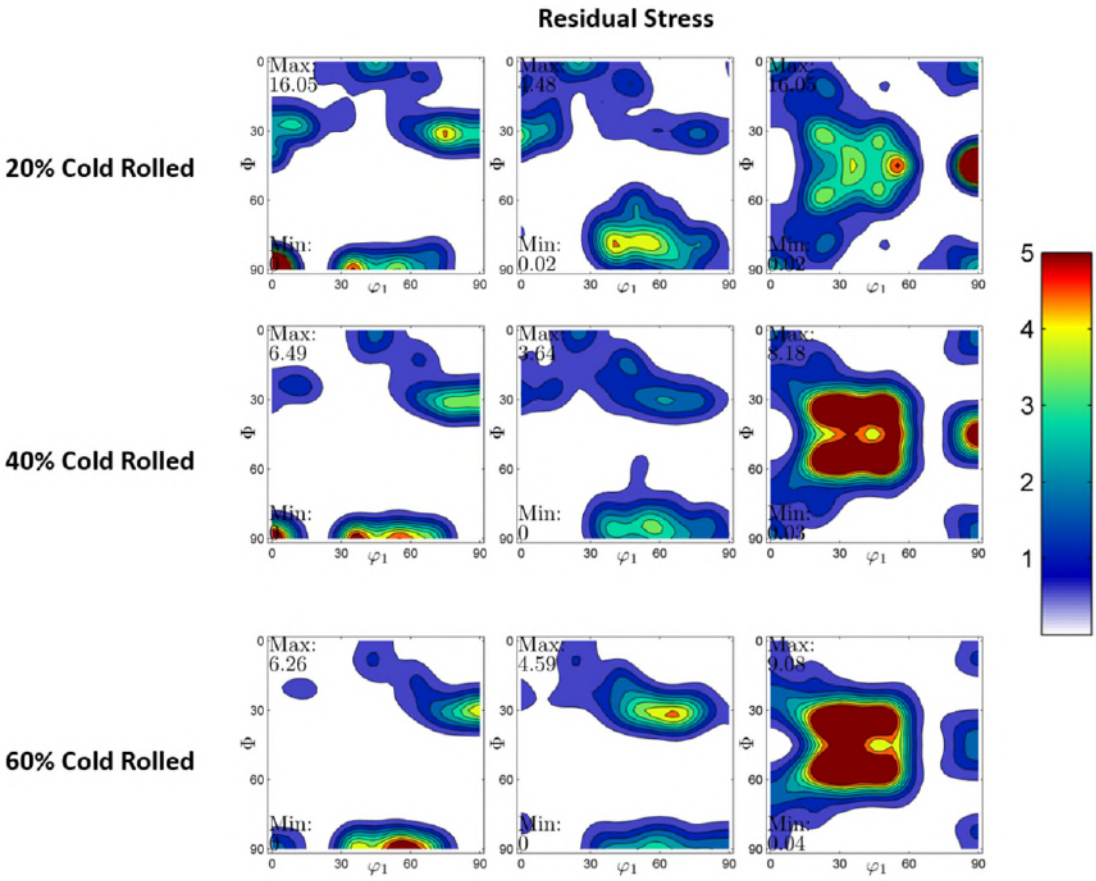

Fig 9: Residual stress orientation distribution function in plane strain compression

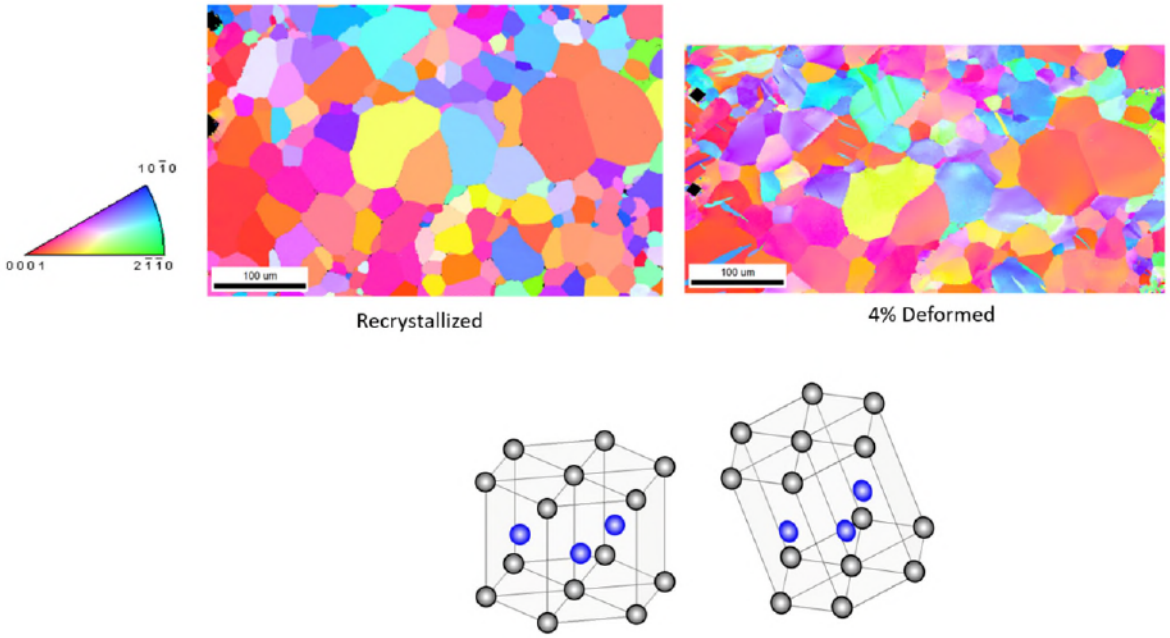

Fig 10: Microstructure evolution with plastic deformation

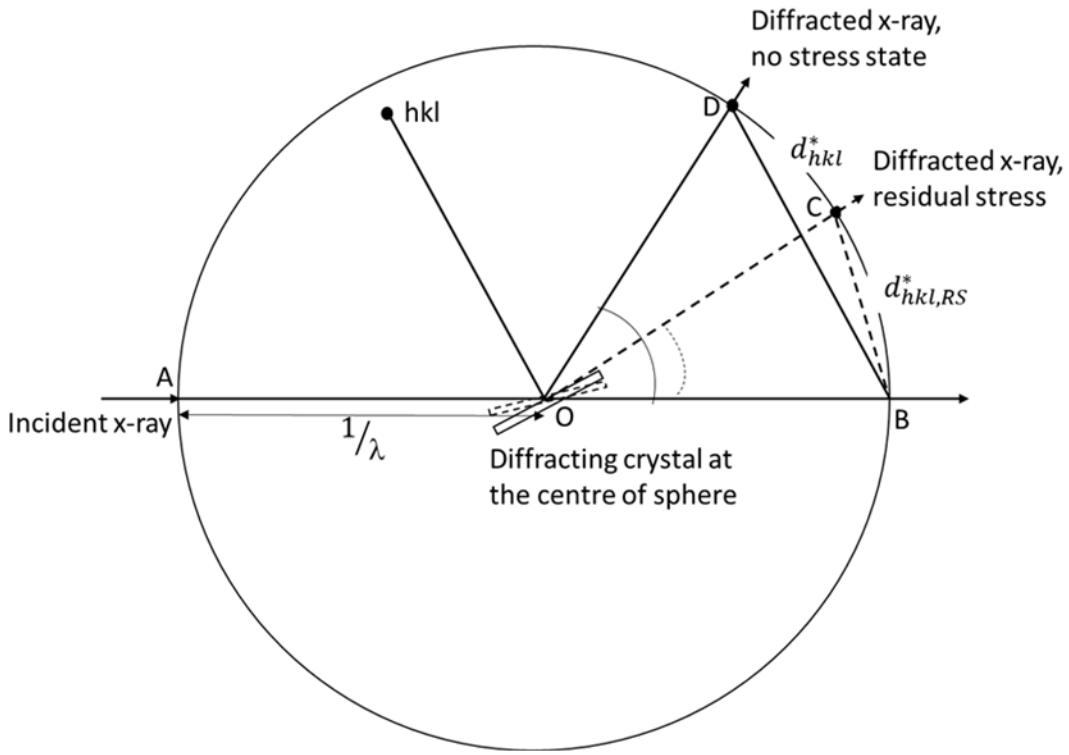

Fig 11: Ewald sphere reconstruction due to residual stress development

Cranfield University

CERES https://dspace.lib.cranfield.ac.uk

School of Aerospace, Transport and Manufacturing (SATM) Staff publications (SATM)

2022-03-07

X-ray diffraction for the determination of residual stress of crystalline material: an overview

Lodh, Arijit

Springer

Lodh A, Thool K, Samajdar I. (2022) X-ray diffraction for the determination of residual stress of crystalline material: an overview, Transactions of the Indian Institute of Metals, Volume 75, Issue 4, April 2022, pp. 983-995

https://doi.org/10.1007/s12666-022-02540-6

Downloaded from Cranfield Library Services E-Repository